Generation of Sum and Difference Radiation Beam with a 2-bit Polarization-Dependent Metasurface

Mei, Peng; Pedersen, Gert Frølund; Zhang, Shuai

Published in:
2022 16th European Conference on Antennas and Propagation (EuCAP)

DOI (link to publication from Publisher):
10.23919/EuCAP53622.2022.9769559

Publication date:
2022

Document Version
Accepted author manuscript, peer reviewed version

Generation of Sum and Difference Radiation Beams with a 2-bit Polarization-Dependent Metasurface

Peng Mei[1], Gert Frølund Pedersen[1], Shuai Zhang[1]
[1] Antennas, Propagation, and Millimeter-Wave Systems (APMS) section, Department of Electronic Systems, Aalborg University, Aalborg, 9000, Denmark, mei@es.aau.dk, gfp@es.aau.dk, sz@es.aau.dk

***Abstract*— This paper describes the generation of sum and difference radiation beams with a 2-bit polarization-dependent (PD) metasurface. A single-layer and cross-shaped dipole unit cell is proposed to implement the PD metasurface. By appropriately optimizing the dimensions of the unit cell, it is readily able to offer a 2-bit reflection phase for two orthogonal (horizontal and vertical) polarizations independently. A horn antenna is adopted as the feed source to illuminate the PD metasurface. Sum and difference radiation beams can be achieved when the phase shifts of the PD metasurface are appropriately imposed in horizontal and vertical polarizations by mechanically rotating the PD metasurface 90 degrees. For demonstration, a circular PD metasurface composed of 232 unit cells is implemented at the millimeter-wave band. The simulations reveal that the PD metasurface-based scheme can offer stable sum and difference radiation beams from 24 to 28GHz, where the null depth levels at broadside direction are all below -20dB. The gains of the sum and difference radiation beams are 23.6dBi and 22.1dBi at 26GHz, respectively.**

***Index Terms*—Millimeter-wave, polarization-dependent, phase quantization, sum and difference, null depth.**

I. INTRODUCTION

Monopulse antennas capable of offering sum and difference radiation beams have been widely used due to their exceptional angle estimation abilities for target localization and tracking in radar communication systems [1]. The conventional technologies enabling sum and difference radiation beams of monopulse antennas were to employ comparator-based waveguides to illuminate the Cassegrain parabolic surface [2]-[4]. There were usually several ports in the monopulse antennas, each of which was responsible for a certain radiation beam (sum radiation beam in E- or H-plane, difference radiation beam in E- or H-plane). Therefore, the sum and difference radiation beams of such monopulse antennas can be switched by exciting the corresponding ports. For sake of low profiles, some planar-antenna-array-based monopulse antennas have been developed to offer sum and difference radiation beams [5]-[9]. In general, the planar monopulse antennas consist of two parts, e.g., radiating elements and feeding networks, where the feeding networks are essential to generate the sum and difference radiation beams. Note that the complexity of the feeding network highly relies on the amounts of the sum and difference radiation patterns. Specifically speaking, the feeding network was relatively simple when the monopulse antennas only offer sum and difference radiation beams in E- or H-plane [7]-[9]. By contrast, it will be complicated if the sum and difference radiation beams are preferred in both E- and H-plane [5], [6]. What's more, more antenna elements are needed if a high gain is desired, therefore resulting in the higher complexity of the corresponding feeding network accordingly. The complicated feeding network unavoidably lowers the total efficiencies of the monopulse antennas especially at the millimeter-wave or even higher frequency bands. On the other hand, one of the defects of the planar monopulse antennas lies in the narrow bandwidth. The authors, for example, proposed a SIW-based planar array antenna with sum and difference radiation beams solely in one plane, the bandwidth of the monopluse antenna was only 1.2% [9].

In this paper, a simple scheme is proposed to generate sum and difference radiation beams with a polarization-dependent (PD) metasurface. To simplify the design of the PD metasurface and still maintain its performance (e.g., aperture efficiency, etc.), a 2-bit PD unit cell is properly designed and optimized to implement the PD metasurface, offering the desired phase shifts to enable sum and difference radiation beams in horizontal and vertical polarizations respectively when the PD metasurface is illuminated by a feed source. With the polarization of the feed source fixed, sum and difference radiation beams can be readily achieved by simply rotating the PD metasurface 90 degrees. The simulations demonstrate that the PD metasurface-based scheme can provide stable sum and difference radiation beams from 24 to 28GHz, where the null depth levels at broadside direction are all below -20dB.

II. POLARIZATION-DEPENDENT METASURFACE SCHEME

This section describes the scheme to generate sum and difference radiation beams with a polarization-dependent metasurface. Fig. 1 depicts the schematic diagram of the proposed scheme that geometrically resembles a reflectarray antenna, consisting of a feed source and a metasurface. The strategy to generate sum and difference radiation beams here is to rotate the metasurface 90 degrees with the polarization of the feed source fixed. This requires the metasurface can offer independent and desired phase shifts in horizontal and vertical polarizations to generate the sum and difference radiation beams.

For a sum radiation beam, the unit cells of the metasurface should offer proper phase shifts to compensate for the geometrical path differences from the phase center of the feed source to the unit cells of the metasurface, converting the spherical waves from the feed source to (quasi-) plane

waves. By contrast, an extra phase gradient should be imposed on unit cells of the metasurface for the sake of a difference radiation beam. Fig. 2 demonstrates the possible phase distributions to generate sum and difference radiation beams with an example of a 16-element linear antenna array. It can achieve a sum (focused) beam as shown in Fig. 2(a) when all antenna elements are in phase. One of the solutions to generate a difference radiation beam is uniformly dividing the linear antenna array into two clusters, where the two clusters have a 180 phase difference as shown in Fig. 2(b).

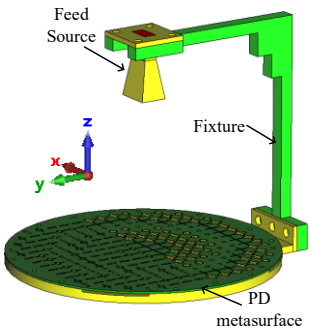

Fig. 1. The schematic diagram of the proposed scheme to generate sum and difference radiation beams.

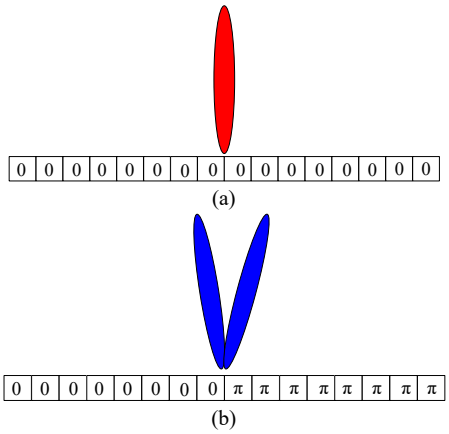

Fig. 2. Phase distributions to generate sum and difference radiation beams. (a). Sum radiation beam. (b). Difference radiation beam.

For the proposed scheme shown in Fig. 1, the phase distributions on the surface of the metasurface are examined and specified to generate sum and difference radiation beams. For demonstration, the periodicity of the unit cell is 6mm that is around half-wavelength at 26GHz, the diameter of the metasurface is 112mm (including the margin area for assembling) with 232 unit cells. The distance between the phase center of the feed source and the metasurface is 64mm. Figs. 3(a) and (b) plot the desired phase distributions on the surface of the metasurface to achieve sum and difference radiation beams, where the strategy to generate the difference radiation beam refers to Fig. 2(b). The circular metasurface is symmetrically divided into two parts along the *y*-axis, where the two parts are imposed a 180 phase difference. To satisfy the simultaneous phase distributions shown in Figs. 3(a) and (b) in horizontal and vertical (two orthogonal) polarizations, the metasurface should be polarization-dependent (PD) so that the reflection phases can be independently controlled in horizontal and vertical polarizations. To simplify the implementation of the PD metasurface and maintain its performance at the same time, a 2-bit phase quantization is adopted here, which has been turned out to offer comparable performance in terms of bandwidth, realized gain, aperture efficiency, etc. compared with the continuous phase shift [10]-[12]. Figs. 3(c) and (d) give the desired 2-bit phase distributions on the surface of the PD metasurface by discretizing the continuous phase distributions shown in Figs. 3(a) and (b).

According to the phase distributions in Figs. 3(c) and (d), the desired phase shifts in horizontal and vertical polarizations on each unit cell pixel can be obtained. It is found that only eight phase shift combinations are needed to implement the desired PD metasurface as tabulated in Tab. I. Once the PD metasurface is determined, the sum and difference radiation beam can be achieved by simply rotating the PD metasurface 90 degrees.

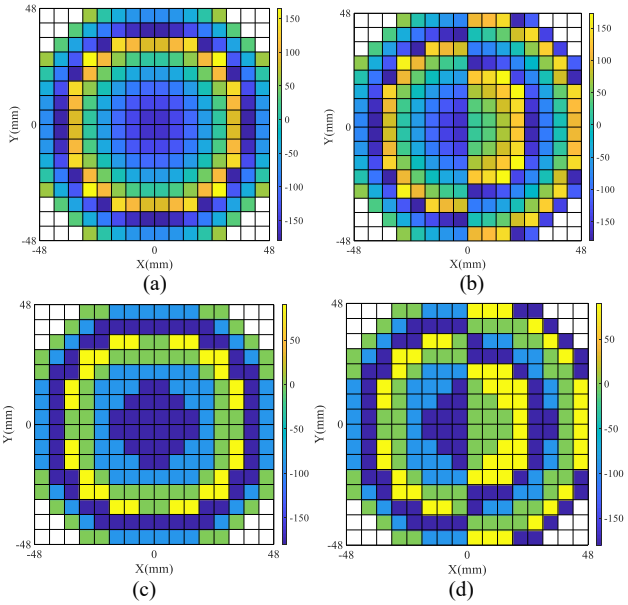

Fig. 3. Phase distributions on the surface of the PD metasurface at 26GHz. (a). Sum radiation beam (continuous phase shifts). (b). Difference radiation beam (continuous phase shifts). (c). Sum radiation beam (2-bit phase shifts). (d). Difference radiation beam (2-bit phase shifts).

Tab. I. The desired phase shift combinations to implement the PD metasurface for sum and difference radiation beams.

Vertical polarization	Horizontal polarization
-90°	-90°
-90°	90°
-180°	-180°
-180°	0°
0°	0°
0°	-180°
90°	-90°
90°	90°

III. IMPLEMENTATIONS AND SIMULATIONS

This section will first focus on designing a unit cell capable of offering the reflection phases in horizontal and vertical polarizations as listed in Tab. I. The PD metasurface is then implemented with the unit cells, its performance to generate sum and difference radiation beams is evaluated with CST Microwave Studio software.

A. Unit cell design.

Fig. 4 presents the geometry of the polarization-dependent unit cell. A cross-shaped dipole is printed on the Rogers 4003C substrate with a thickness of 0.813mm, a dielectric constant of 3.55, and a loss tangent of 0.0027. The substrate floats above a metal ground with an air spacer of h as shown in Fig. 1(b). The periodicity of the unit cell (a) and air spacer (h) are 6 and 1mm to make the unit cell work in the frequency range of interest (24 to 28GHz). The periodic boundary condition is imposed on the unit cell in CST software to mimic an infinite surface.

For the proposed unit cell shown in Fig. 4, it can offer distinct reflection phases for horizontal (x-) and vertical (y-) polarized incidence waves by tuning the dimensions of (l_1, w_1) and (l_2, w_2) separately. The dimensions of (l_1, w_1) and (l_2, w_2) are determined and summarized in Tab. II after performing some simulations to offer the desired reflection phases listed in Tab. I. For brevity, the reflection phases versus frequencies are presented as shown in Fig. 5 when the PD unit cell provides the first four reflection phases in horizontal (x-polarization) and vertical (y-polarization) polarizations in Tab. II. As seen in Fig. 5, the PD can offer the desired reflection phases in horizontal and vertical polarizations from 24 to 28 GHz.

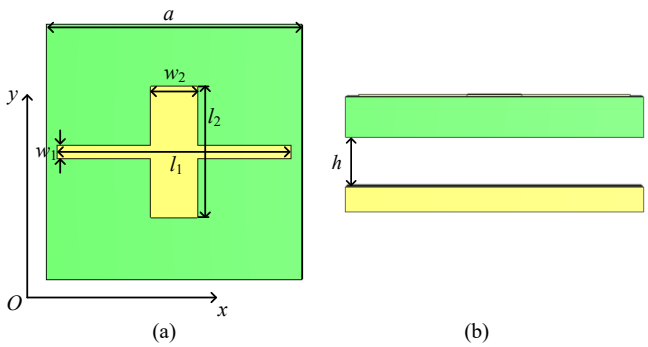

Fig. 4. The geometry of the polarization-dependent unit cell. (a). Front view. (b). Side view. (a = 6mm, h = 1.0mm)

Tab. II. The dimensions of the cross-shaped dipole correspond to the desired reflection phases.

Horizontal ~ Vertical polarization	Dimensions (mm)
-90° ~ -90°	l_1 = 1.5, w_1 = 1.0; l_2 = 1.5, w_2 = 1.0
-90° ~ 90°	l_1 = 4.16, w_1 = 0.9; l_2 = 0.9, w_2 = 0.9
-180° ~ -180°	l_1 = 3.3, w_1 = 1.5; l_2 = 3.3, w_2 = 1.5
-180° ~ 0°	l_1 = 6.0, w_1 = 0.3; l_2 = 3.08, w_2 = 1.1
0° ~ 0°	l_1 = 6.0, w_1 = 0.3; l_2 = 6.0, w_2 = 0.3
0° ~ -180°	l_1 = 3.08, w_1 = 1.1; l_2 = 6.0, w_2 = 0.3
90° ~ -90°	l_1 = 0.9, w_1 = 0.9; l_2 = 4.16, w_2 = 0.9
90° ~ 90°	l_1 = 5.5, w_1 = 1.5; l_2 = 5.5, w_2 = 1.5

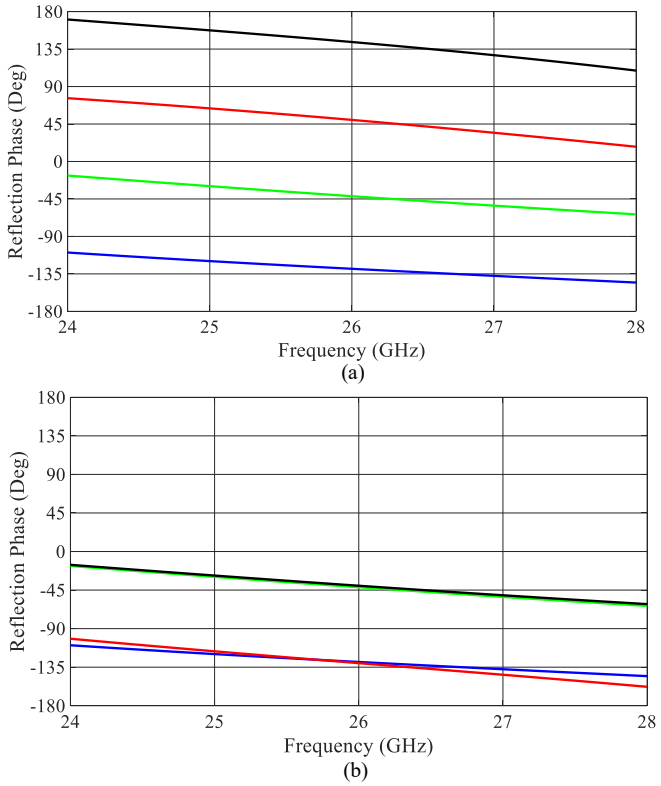

Fig. 5. Simulated reflection phases of the PD unit cell with different values of (l_1, w_1) and (l_2, w_2). (a). Horizontal (x-) polarized normal incidence wave. (b).Vertical (y-) polarized normal incidence wave. (Black: l_1 = 4.16mm, w_1 = 0.9mm, l_2 = 0.9mm, w_2 = 0.9mm; Red: l_1 = 6.0mm, w_1 = 0.3mm, l_2 = 3.08mm, w_2 = 1.1mm; Green: l_1 = 1.5mm, w_1 = 1.5mm, l_2 = 1.5mm, w_2 = 1.5mm; Blue: l_1 = 3.3mm, w_1 = 1.5mm, l_2 = 3.3mm, w_2 = 1.5mm.)

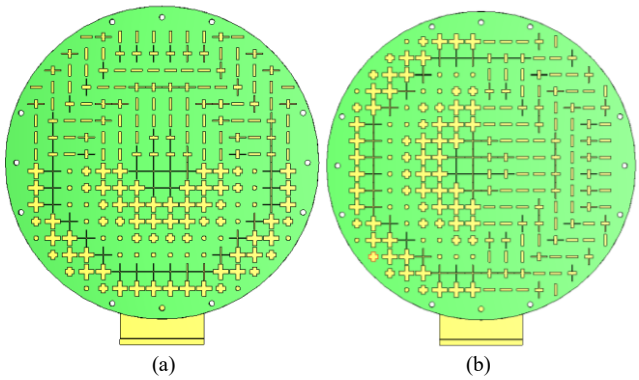

Fig. 6. The patterns of the metasurface to generate sum and difference radiation beams. (a). Sum radiation beam. (b). Difference radiation beam. (The feed sources are invisible, and have the same polarizations. Only the PD metasurface rotates 90 degrees from (a) to (b)).

B. Implementations of the 2-bit polarization-dependent metasurface and simulations of sum and difference radiation beams.

According to the phase distributions shown in Figs. 3(c) and (d), and the relation between the dimensions and the reflection phases listed in Tab. II, the PD metasurface is then implemented. Fig. 6 presents the respective patterns of the metasurface to generate sum and difference radiation

beams. The reflection coefficients of the PD metasurface-based scheme are simulated and presented in Fig. 7 with sum and difference radiation beams, where -10dB reflection coefficients can be observed from 24 to 28GHz. The radiation patterns of the PD metasurface-based scheme at 26GHz are simulated and plotted in Fig. 8, where sum and difference radiation beams are observed. The realized gains of the sum and difference radiation beams are 23dBi and 21.3dBi, respectively. The null depth level of the difference radiation beam is around -20dB. As seen in Fig. 8, the cross-polarization levels of sum and difference radiation beams are below -20 and -30dB, respectively.

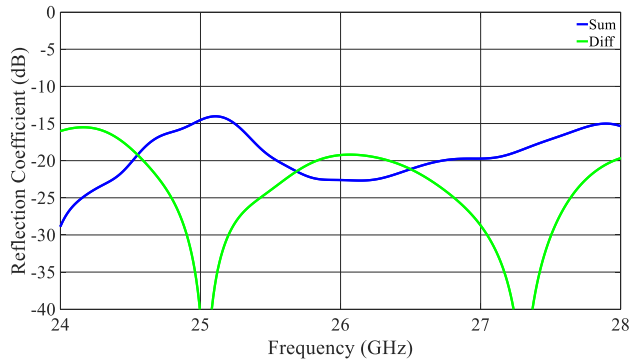

Fig. 7. Simulated reflection coefficients of the PD metasurface-based scheme with sum and difference radiation beams.

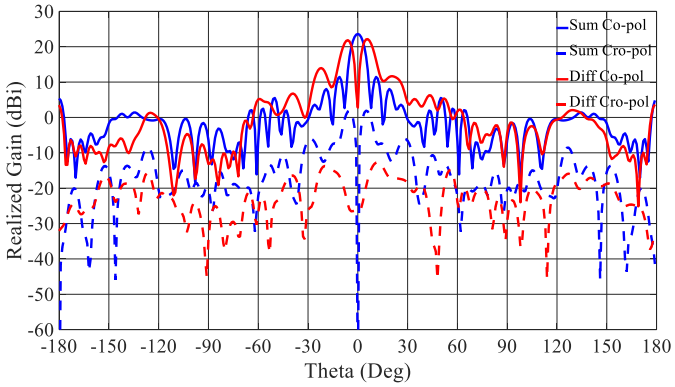

Fig. 8. Simulated sum and difference radiation beams of the PD metasurface-based scheme at 26 GHz.

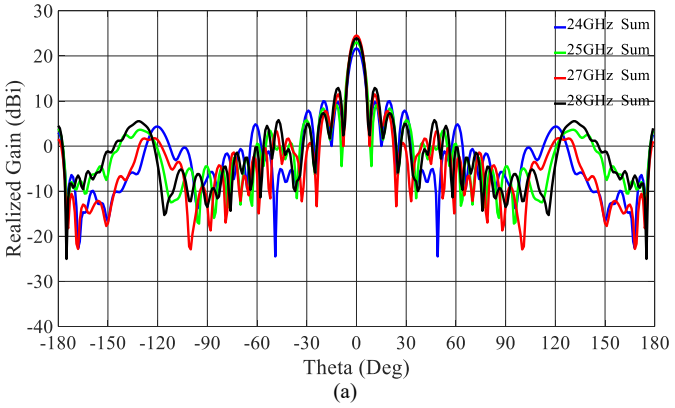

(a)

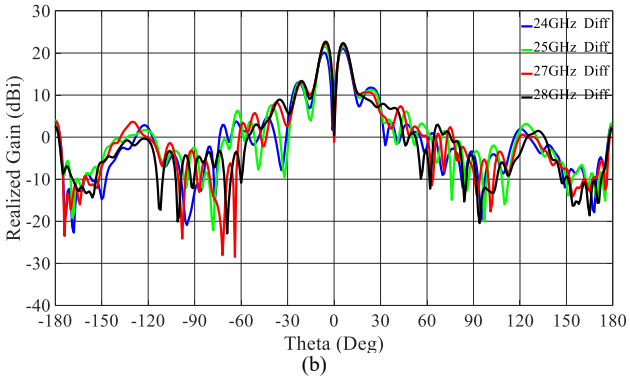

(b)

Fig. 9. Simulated sum and difference radiation beams of the PD metasurface-based scheme at 24, 25, 27, and 28 GHz. (a). Sum radiation beams. (b). Difference radiation beams.

Fig. 9 plots the simulated radiation patterns of the PD metasurface-based scheme at 24, 25, 27, and 28GHz, where sum and difference radiation patterns are still observed. The null depth levels at broadside directions are below -20dB. The results shown in Figs. 8 and 9 demonstrate the stable and wideband performance of the PD metasurface-based scheme in terms of enabling sum and difference radiation beams.

It should be mentioned here the difference radiation beam can also be modified by adopting other sequential of 0 and π shown in Fig. 2(b), e.g., (0, π, 0, π, …, 0, π, 0, π) or (0, 0, π, π, …, 0, 0, π, π), where the pointing directions of the difference beam and the null depth levels can be controlled. This paper demonstrates the difference radiation beam solely in H-plane. However, the proposed 2-bit PD metasurface-based scheme can also achieve the difference radiation beams in solely E-plane, or both E- and H-plane, or both +/- 45degrees planes when the phase distributions on the surface of the 2-bit PD metasurface are properly imposed. The corresponding results will be presented at the Conference.

IV. CONCLUSIONS

This paper describes a simple scheme to generate sum and difference radiation beams using polarization-dependent metasurface. A 2-bit phase quantization is adopted to simplify the design of the PD metasurface and still maintain its performance. The PD metasurface is properly designed to offer the desired reflection phases in horizontal and vertical polarizations. A horn antenna is used to illuminate the PD metasurface. Sum and difference radiation beams can be obtained by simply rotating the PD metasurface 90 degrees with the polarization of the horn antenna fixed. The simulations demonstrate the proposed PD metasurface-based scheme can provide stable sum and difference radiation beams from 24 to 28GHz within which the null depth levels at broadside direction are all below -20dB.

The scheme described in this paper could be served as an alternative solution to enable sum and difference radiation beams due to its simple configuration, low loss, and wide bandwidth.

ACKNOWLEDGMENT

This work was supported by the RANGE and MARSS projects.

REFERENCES

[1] S. M. Sherman, *Monopulse Principles and Techniques*. Dedham, MA, USA: Artech House, 1984.

[2] P. W. Hannan, "Optimum feeds for all three modes of a monopulse antenna I: Theory," *IRE Trans. Antennas Propag*., pp. 444-454, Sep. 1961.

[3] P. Zhang, G. Zhao, S. Xu, F. Yang, and H. Sun, "Design of a W-band full-polarization monopulse Cassegrain antenna," *IEEE Antennas Wireless Propag Letts*., vol. 16, pp. 99-103, 2017.

[4] J. Zhao, H. Li, X. Yang, W. Mao, B. Hu, T. Li, H. Wang, Y. Zhou, and Q. Liu, "A compact Ka-band monopulse Cassegrain antenna based on reflectarray elements," *IEEE Antennas Wireless Propag Letts*., vol. 17, no, 2, pp. 193-196, Feb. 2018.

[5] H. Wang, D. G. Fang, and X. Chen, "A compact single layer monopulse microstrip antenna array," *IEEE Trans. Antennas Propag*., vol. 54, no. 2, pp. 503-509, Feb. 2006.

[6] J. Zhu, S. Liao, S. Li, and Q. Xue, "60GHz substrate-integrated waveguide-based monopulse slot antenna arrays," *IEEE Trans. Antennas Propag*., vol. 66, no. 9, pp. 4860-4865, Sep. 2018.

[7] Y. Wang, G. Wang, Z. Yu, J. Liang, and X. Guo, "Ultra-wideband E-plane monopulse antenna using Vivaldi antenna," *IEEE Trans. Antennas Propag*., vol. 62, no. 10, pp. 4961-4969, Oct. 2014.

[8] T. Yang, Z. Zhao, D. Yang, X. Liu, and Q. Liu, "A single-layer SIW slots array monopulse antenna excited by a dual-mode resonator," *IEEE Access*, vol. 7, pp. 131282-131288, 2019.

[9] H. Chu, J. Chen, S. Luo, and Y. Guo, "A millimeter-wave filtering monopulse antenna array based on substrate integrated waveguide technology," *IEEE Trans. Antennas Propag*., vol. 64, no. 1, pp. 316-321, Jan. 2014.

[10] P. Mei, G. F. Pedersen, and S. Zhang, "A broadband and FSS-based transmitarray antenna for 5G millimeter-wave applications," vol. 20, no. 1, pp. 103-107, Jan. 2021.

[11] Y. Ge, C. Lin, and Y. Liu, "Broadband folded transmitarray antenna based on an ultrathin transmission polarizer," *IEEE Trans. Antennas Propag*., vol. 66, no. 11, pp. 5974-5981, Nov. 2018.

[12] K. Mavrakakis, H. Luyen, J. Booske, and N. Behdad, "Wideband transmitarrays based on polarization-rotating miniaturized-element frequency selective surfaces," *IEEE Trans. Antennas Propag*., vol. 68, no. 3, pp. 2128-2137, Mar. 2020.